Kent Academic Repository

Full text document (pdf)

Citation for published version

Adabi, Saba and Fotouhi, Audrey and Xu, Qiuyun and Daveluy, Steve and Mehregan, Darius and Podoleanu, Adrian G.H. and Nasiriavanaki, Mohammadreza (2017) An overview of methods to mitigate artifacts in optical coherence tomography imaging of the skin. Skin Research and Technology . ISSN 0909-752X.

DOI

https://doi.org/10.1111/srt.12423

Link to record in KAR

http://kar.kent.ac.uk/64638/

Document Version

Author's Accepted Manuscript

An Overview of Methods to Mitigate Artefacts in Optical Coherence Tomography Imaging of the Skin

Saba Adabi [a,b], Audrey Fotouhi [c], Qiuyun Xu [a], Steve Daveluy [d,f], Darius Mehregan [d], Adrian Podoleanu [e] and Mohammadreza Nasiriavanaki * [a,d,f]

[a] Wayne State University, Department of Biomedical Engineering, Engineering Faculty 818 W. Hancock, Detroit, Michigan, USA,
[b] Roma Tre University, Engineering Faculty, Department of Applied Electronics, Via.V.Voltera, Rome, Italy, 00146
[c] Wayne State University School of Medicine, Detroit, Michigan, USA
[d] Department of Dermatology, Wayne State University School of Medicine, Detroit, Michigan, USA
[e] School of Physical Sciences, Applied optics group, University of Kent, Canterbury, Kent, United Kingdom
[f] Barbara Ann Karmanos Cancer Institute, Detroit, Michigan, USA

*Corresponding author: Mohammadreza Nasiriavanaki

Address: 818 W Hancock street, Detroit 48207 MI

Email: mrn.avanaki@wayne.edu

Background: Optical Coherence Tomography (OCT) of skin delivers three dimensional images of tissue microstructures. Although OCT imaging offers a promising high resolution modality, OCT images suffer from some artefacts that lead to misinterpretation of tissue structures. Therefore, an overview of methods to mitigate artefacts in OCT imaging of the skin is of paramount importance. Speckle, intensity decay, and blurring are three major artefacts in OCT images. Speckle is due to the low coherent light source used in the configuration of OCT. Intensity decay is a deterioration of light with respect to depth, and blurring is the consequence of deficiencies of optical components.

Method: Two speckle reduction methods (one based on artificial neural network and one based on spatial compounding), an attenuation compensation algorithm (based on Beer-Lambert law) and a de-blurring procedure (using deconvolution) are described. Moreover, optical properties extraction algorithm based on extended Huygens–Fresnel (EHF) principle to obtain some additional information from OCT images are discussed.

Results: In this short overview, we summarize some of the image enhancement algorithms for OCT images which address the abovementioned artefacts. The results showed a significant improvement in the visibility of the clinically relevant features in the images. The quality improvement was evaluated using several numerical assessment measures.

Conclusion: Clinical dermatologists benefit from using these image enhancement algorithms to improve OCT diagnosis and essentially function as a non-invasive optical biopsy.

Keywords: Optical Coherence Tomography, Image Enhancement, Speckle Reduction, Blurring Correction, Intensity Decay Compensation.

1. INTRODUCTION

In dermatology, the gold standard for diagnosis of a disease is a biopsy that is sent for histopathological examination [1]. There is still no reliable or definitive method of non-invasive diagnosis for skin disease. Histopathology requires slicing and staining a sample, physically altering it each time it is stained [2]. This method leaves room for human error, through slicing, staining, and reading the image. In addition, biopsy can be traumatic and risky, especially for elderly patients, because of poor wound healing and possibility of infection [3]. Therefore, several non-invasive imaging modalities have been developed to enhance the diagnosis of skin diseases [4-10]. Among several different modalities, optical coherence tomography (OCT) stands out. When compared with multispectral digital dermoscopy and spectroscopy, for example, it is noted that these techniques lack adequate penetration depth [11-14]. Another technique, high frequency sonography has a better penetration depth, however the contrast is not satisfactory [15]. OCT's intermediate resolution and penetration depth give it great potential to image the skin. Recently, OCT has been used as an optical biopsy method for differentiation among different tissues, e.g., healthy versus tumorous [16,17].

OCT is a non-invasive, non-ionizing optical imaging modality which works based on low coherence interferometry [18,19]. To form an OCT image, the magnitude and time delay of backscattered infrared light returned from a biological sample is measured transversally [20,21]. Providing high resolution images and a moderate penetration depth, i.e., one to three millimeters, OCT is currently utilized in several medical and biomedical applications including dermatology, dentistry [22], oncology [23], and cardiology [24] in addition to its initial successes in ophthalmology [25]. Quantitative analysis of OCT images through extraction of optical properties has made OCT an even more powerful modality [26-28]. An OCT system is characterized by several parameters such as imaging speed, lateral and axial resolutions, and penetration depth [29]. To assess these system parameters, a virtual tissue, so-called phantom, with known optical properties, e.g., anisotropy factor, absorption and scattering coefficients, is utilized [30-32]. The phantoms are usually designed using Mie theory where the concentration and particle size of scatterers and absorbers are determined.

OCT imaging is a favorable high-resolution imaging method in medical and biomedical applications, and many modifications have already been applied on the OCT hardware and software, however, OCT images still contain artefacts [29,33-35]. Three major artefacts in OCT images are speckle noise, intensity decay and blurring. Similar to other low coherent imaging modalities, OCT images are contaminated by speckle which degrades the quality of images and conceals diagnostically relevant features. Intensity decay is due to the decline in the incident and backscattered light amplitude when it passes through the biological sample [18]. Blurring is a result of aberrations and is due to the imperfection of optical devices used in the configuration of the OCT [36] as well as aberrations introduced by superficial layers of the tissue investigated. Blurring mainly deteriorates the lateral resolution of OCT images. Addressing these issues, OCT images need to be enhanced in order to deliver microscopic features of biological samples more effectively. In this manuscript, some of the most significant image artifacts in OCT imaging and the advancements to mitigate them are reviewed; specifically speckle noise, intensity decay and blurring. A speckle reduction method, an attenuation compensation algorithm and a de-blurring procedure are described. Moreover, optical properties extraction routines to obtain some additional information from OCT images are discussed.

Enhancement of the quality of images in combination with assessment of optical properties can enhance the feasibility of differentiation of melanoma from benign lesions [37] as well as the differentiation of subtypes of basal cell carcinoma [37].

2. LOW COHERENCE INTERFEROMETRY

An OCT image is constructed based on the principles of time of flight and low coherence interferometry [38]. The interferometry is used to magnify the small time delay between the backscattered light returned from the sample and the reflected light from a reference mirror (Fig.1). The basic components of an OCT system are a low coherent light source, with a short enough coherence length to be able to have depth sectioning capability, a beam splitter to split light between two arms; a reference mirror, and some opto-electronic components such as a XY galvo scanner [39]. Coherence length is a measure of temporal coherence, expressed as the propagation distance over which the coherence significantly decays. The schematic of a time domain OCT system is shown in Fig.1.

3. SPECKLE REDUCTION

In OCT imaging, if the central wavelength of the light source is equal to or larger than the compartments within the sample under investigation, the interference of the reflected light with different amplitudes and phases generates a grainy texture in the image called speckle. Speckle degrades the quality of OCT images, particularly the borders of cellular layers [40] in comparsion with speckle-free imaging methods [41]. The probability density function (PDF) of the speckle has been approximated by Rayleigh distribution, or Rician distribution [42]. Speckle pattern is highly dependent on the microstructural content (size and density) of the sample being imaged. Due to this correlation, speckle is also known to carry some morphological information, thus is not appropriate to consider it as an image noise. This issue has made finding a suitable solution to reduce the speckle quite challenging. The speckle reduction methods are categorized into two main categories: software based and hardware methods [26,40,43-53].

3.1 Software-Based Speckle Reduction Methods; Digital Filtering

Software based speckle reduction methods rely on a mathematical model of the speckle, and they can be classified into adaptive and non-adaptive filters. The former are implemented based upon the local first order statistics, such as mean and variance, while the latter are implemented based on the overall statistics in the image. Wiener filter is one of the most popular adaptive methods [54,55]. Some of the non-adaptive algorithms are Kuwahara filter, Hybrid Median filter, Enhanced LEE filter (ELEE), Symmetric Nearest Neighborhood (SNN), thresholding with fuzzy logic [56,57]. Wavelet based de-speckling has been a successful non-adaptive de-speckling method in which the image is decomposed into its wavelet bases, allowing differentiation of noise components through signal processing [29,50,58-60]. Considering the importance of wavelet mother function in this method, Haar mother function has proven a fast and efficient solution, enabling speckle noise reduction without substantially diminishing contrast or spatial resolution in the image [61,62]. Another adaptive speckle reduction method has been developed based on artificial neural network (ANN) [63,64]. ANN offers an intelligent solution which reduces speckle while preserving the morphological information in the image. In this method, the speckle is first modelled. The model used [65-67] follows Rayleigh distribution and is given by Eq.1:

$$\boldsymbol{f(x_{i,j})} = \frac{x_{i,j}e^{\frac{-x_{i,j}^2}{2\sigma^2}}}{\sigma^2} \qquad (1)$$

where $x_{i,j}$ is the image pixel and σ is the noise variance of the image (noise parameter). A cascade forward back propagation ANN is then used to estimate a noise parameter for the image, followed by a numerical solution to the inverse Rayleigh distribution function [68]. The block diagram of this algorithm is illustrated in Fig. 2. C-scan (en-face) OCT images of Drosophila heart before and after applying ANN based de-speckling method are presented in Fig. 3.

3.2 Hardware-based speckle reduction methods; Compounding techniques

The most common hardware-based speckle reduction method is compounding. In compounding techniques [69], partially de-correlated images acquired from a stationary sample are averaged. The quantities to be averaged specify the compounding procedure.

Some of the quantities used in compounding methods are backscattering angles, central wavelengths, polarizations, and displacements. This results in techniques referred to as angular compounding, frequency compounding, polarization compounding, and spatial compounding, respectively [18,46,70,71].

For instance, in the spatial compounding method, the averaging quantity is the tissue or the imaging probe motion, which comes from the inherent imperfection of the scanners used in the configuration of the imaging system [72]. Five different algorithms including averaging, random weighted averaging, random pixel selection and random pixel selection together with median filtering were used to average their partially correlated images obtained from the spatial compounding method [72]. The flowchart of the spatial compounding method with different algorithms is illustrated in Fig. 4.

The authors demonstrated that the random pixel selection together with median filtering represent an efficient, simple, and edge-preserving de-speckling method compared to the common averaging method [72].

4. IMAGE BLURRING CORRECTION

Blurring stems from wavefront aberration in the imaging system [73,74]. Aberrations are produced by the imperfections of optical devices that are used in the interface optics of the imaging system. They result in resolution and contrast degradations. One way to reduce aberration is by adaptive optics (AO). AO systems are composed of a wavefront sensor (WFS) to measure the wavefront distortion, a deformable mirror (DM), or a spatial light modulator (SLM) to correct the distortion, and a control loop algorithm to control the correction process [75]. Recently, less-expensive sensor-less AO methods utilizing blind optimization have been studied [76-78]. In a sensor-less AO system, an optimization algorithm with a cost function, e.g. photo-detected intensity value, is used. Improving the cost function means reducing the aberrations and diminishing the blurriness in the images. Some of the effective optimization methods used in sensor-less AO systems are simulated annealing algorithm (SA), genetic algorithm (GA), and particle swarm optimization (PSO) [79]. Avanaki et al. compared the performance of these three optimization methods in a sensor-less AO systems [80]. Another popular method to reduce blurriness is deconvolution. Several deconvolution techniques have been studied [81-85]. For some deconvolution methods, the point spread function (PSF) of the imaging system needs to be determined. There are two main methods to obtain the PSF; (a) analytical methods, (b) imaging very small particles embedded in a solid phantom. Fish et al. successfully used the Lucy–Richardson algorithm, which is a well-established deconvolution algorithm, to deblur OCT images [86,87]. Lucy–Richardson algorithm is based on the maximum-likelihood calculation to recover an undistorted image which has been blurred by a known PSF [87]. In Fig.5, the result of using deconvolution algorithm on an image of skin is shown.

5. INTENSITY DECAY COMPENSATION

On OCT image, several layers and structures of the skin are distinguishable [16]. The stratum corneum, or top keratin-full layer of the epidermermis is visible as a hyperreflective line at the skin-air interface. The other epidermal layers can sometimes be visualized depending on the location being imaged. The dermal-epidermal junction, which is disrupted in many skin diseases and cancers, is visualized as a junction between a less intense signal area (epidermis) and more intense signal area (dermis). The dermis is seen as an area of intense signal with hyporeflective patches, which are hair follicles or sebaceous glands.

The turbidity of biological tissues results in attenuation in the incident light amplitude in relation with the depth of penetration, therefor an attenuation compensation algorithm is required. One way to model light attenuation is to use Monte Carlo simulation [49]. In attenuation compensation of an OCT image, it is beneficial to have prior information about the tissue. The authors modelled the skin based on its layered histological architecture in OCT skin images [57]. They then estimated the attenuation of light in OCT skin images for each layer separately. They segmented the OCT image prior to attenuation estimation or compensation similar to the method in [88]. They assume that the A-lines' intensity profile extrema correspond to different layers [89,90]. When the border between two adjacent layers however is not easily distinguishable, a more complex segmentation algorithm is required [89]. For instance, a semi-automatic segmentation method based on a user defined threshold, has been described by Blomberg. et al. [91]; Hori et al. proposed another segmentation algorithm based on A-scan peaks and some statistical operations [92]. In the mentioned work, rubber-band algorithm along with some interpolations was used to resolve boundary problems.

An attenuation compensation algorithm for OCT images of skin is proposed in [93,94]. In this algorithm, a weighted median filter is used to reduce the speckle. Afterwards, the de-noised image is used as the input to a skin layer detection algorithm that searches for the most probable position of local extrema along A-scans by using a cumulative occurrence profile followed by some morphological operations [68]. The attenuation coefficient is calculated for each layer of skin (creating an attenuation model for skin) using the Beer-Lambert law; Beer-Lambert law relates the total attenuation of the signal with the property of the tissues where light passes through [95]. Compensation is then performed for each layer by using the attenuation coefficient of that layer considering the impact of the upper layers' attenuation. In Fig.6, the image enhancement procedure is demonstrated in a block diagram. The results of attenuation compensation algorithm applied on OCT skin images are demonstrated in Fig.7.

6. OPTICAL PROPERTIES EXTRACTION

An OCT image carries important morphological information. By quantitative analysis of OCT images, some optical properties can be extracted and more information can be delivered to specialists to make diagnostic decisions. Some of the optical properties that can be extracted from OCT images include scattering coefficient, absorption coefficient, refractive index, and anisotropy factor. For instance, with the intention of extracting the scattering coefficient of a region of interest (ROI) on an OCT image, one should refer to the equation of light propagation in tissue. The solution to this equation can be given by using geometric optics approximations, Rytov approximation [96], or extended Huygens–Fresnel (EHF) principle [97-100]. Initial research into optical property extraction and OCT signal modelling is presented by Schmitt, who used single-scattering theory to model the scattering coefficient. He followed up his single scattering model by a modified model for two-layer-scattering geometry [32,101]. Thrane et al. proposed an approach for OCT modelling in a multilayer-scattering geometry based on the ray tracing method, so-called ABCD matrix and the EHF principle [102,103]. They obtained the root mean squared (RMS) of the OCT signal as a function of scattering coefficient, μ_s, at different depths by Eq.2.

$$\langle i^2(z)\rangle = \frac{\alpha^2 P_R P_S \sigma_b}{\pi^2 \omega_H^2}\left[e^{-2\mu_s z} + \frac{2e^{-\mu_s z}(1-e^{-\mu_s z})}{1+\frac{\omega_S^2}{\omega_H^2}} + (1-e^{-\mu_s z})^2\frac{\omega_S^2}{\omega_H^2}\right] \quad (2)$$

where α, is the conversion factor for power to current, P_R and P_S are the optical powers of the reference arm and sample arm beams, respectively. σ_b is the effective backscattering cross section. ω_H^2 and ω_S^2 are the 1/e irradiance radii in the discontinuity plane in the absence and presence of scattering and they are given by to Eqs. 3, 4, and 5,

$$\omega_H^2 = \omega_0^2\left(A-\frac{B}{f}\right)^2 + \left(\frac{B}{k\omega_0}\right)^2 \quad (3)$$

$$\omega_S^2 = \omega_0^2\left(A-\frac{B}{f}\right)^2 + \left(\frac{B}{k\omega_0}\right)^2 + \left(\frac{B}{k\rho_0}\right)^2 \quad (4)$$

ω_0 is 1/e irradiance radius at the lens plane. A and B are elements of the ABCD ray matrix, $k = {2\pi}/{\lambda_0}$ is the wavenumber, λ_0 is the central wavelength of the light source, and f is the focal length of the objective lens. ρ_0, is the lateral coherence length, which is a function of depth and obtained by Eq. (7)

$$\rho_0(z) = \sqrt{\frac{3}{\mu_s z}} \times \frac{\lambda}{\pi\theta_{rms}}\left(\frac{nB}{z}\right) \quad (5)$$

where θ_{rms} is the rms scattering angle. In another study, an optical properties extraction (OPE) algorithm [104] is proposed to compute the scattering coefficient of a ROI in an OCT image [105]. In their OPE algorithm, the averaged A-scan of the ROI between pixel indices ranging through a specified axial depth, was fitted onto equation (4); the distance was minimized using the Levenberg–Marquardt least-square method. Avanaki et al. utilized a dynamic focus (DF)-OCT system in their experiments [106] which made it possible to implement the OPE algorithm much easier. With DF-OCT it was then unnecessary to de-convolve the reflectivity profile from the confocal gate profile. They showed that the scattering coefficients obtained from the OPE algorithm are consistent with those calculated by Mie scattering theory (see Fig.8).
As an applications of the OPE algorithm, they demonstrated differentiation between basal cell carcinoma affected and healthy eyelid tissues via their scattering coefficients extracted by OPE from the OCT images [104,107].

7. CONCLUSION

Optical coherence tomography presents a promising method of non-invasive skin imaging with the potential to supplant biopsy as a diagnostic technique. At this time, diagnosis via OCT relies on the clinician identifying morphologic features of skin disease present in the image. Reducing artefact in the images carries the potential to more accurately discern borders between structures, allowing more accurate diagnosis. Additionally, there is a great deal more information available in the image but beyond the ability of the human eye to discern. Algorithms to extract and analyze the optical properties in OCT images could provide tools to further support the clinician in diagnosis. Image processing and analysis techniques may result in enhanced diagnostic capability for the average dermatologist while providing a more rapid and non-invasive technique.
In this short overview, we summarized three major artefacts in OCT images including speckle, intensity decay and image blurring. The issues are described, along with some of the developed technologies and algorithms to diminish them. Furthermore, optical properties extraction from OCT images and the possibility of using such data to differentiate between healthy and non-healthy tissues is explained.

Acknowledgments

The authors acknowledge the Wayne State University Startup fund.

Conflict of interest

All the authors state no potential conflict of interest.

Ethical approval:

All procedures performed in studies involving human participants were in accordance with the ethical standards of the institutional and/or national research committee and with the 1964 Helsinki declaration and its later amendments or comparable ethical standards.

Informed consent:

Informed consent was obtained from all individual participants included in the study.

References

1. Giavedoni P, Puig S, Carrera C. Noninvasive imaging for nonmelanoma skin cancer. *Seminars in cutaneous medicine and surgery.* 2016;35(1):31-41.
2. Ordonez NG. Value of melanocytic-associated immunohistochemical markers in the diagnosis of malignant melanoma: a review and update. *Human pathology.* 2014;45(2):191-205.
3. Hayashi T, Furukawa H, Kitamura T, et al. Review and proposal of regional surgical management for melanoma: revisiting of integumentectomy and incontinuity dissection in treatment of skin melanoma. *International journal of clinical oncology.* 2017;22(3):569-576.
4. Koehler MJ, Lange-Asschenfeldt S, Kaatz M. Non-invasive imaging techniques in the diagnosis of skin diseases. *Expert opinion on medical diagnostics.* 2011;5(5):425-440.
5. Ghita MA, Caruntu C, Rosca AE, et al. Reflectance confocal microscopy and dermoscopy for in vivo, non-invasive skin imaging of superficial basal cell carcinoma. *Oncology letters.* 2016;11(5):3019-3024.
6. Heredia-Juesas J, Thatcher JE, Yang L, et al. Non-invasive optical imaging techniques for burn-injured tissue detection for debridement surgery. *Conference proceedings : Annual International Conference of the IEEE Engineering in Medicine and Biology Society IEEE Engineering in Medicine and Biology Society Annual Conference.* 2016;2016:2893-2896.
7. Ulrich M, Themstrup L, de Carvalho N, et al. Dynamic Optical Coherence Tomography in Dermatology. *Dermatology.* 2016;232(3):298-311.
8. Thomas G, van Voskuilen J, Truong H, Gerritsen HC, Sterenborg HJ. In vivo nonlinear optical imaging to monitor early microscopic changes in a murine cutaneous squamous cell carcinoma model. *Journal of biophotonics.* 2015;8(8):668-680.
9. Wahrlich C, Alawi SA, Batz S, Fluhr JW, Lademann J, Ulrich M. Assessment of a scoring system for Basal Cell Carcinoma with multi-beam optical coherence tomography. *Journal of the European Academy of Dermatology and Venereology : JEADV.* 2015;29(8):1562-1569.
10. Wald N, Goormaghtigh E. Infrared imaging of primary melanomas reveals hints of regional and distant metastases. *The Analyst.* 2015;140(7):2144-2155.
11. Elbaum M, Kopf AW, Rabinovitz HS, et al. Automatic differentiation of melanoma from melanocytic nevi with multispectral digital dermoscopy: a feasibility study. *Journal of the American Academy of Dermatology.* 2001;44(2):207-218.
12. Gutkowicz-Krusin D, Elbaum M, Jacobs A, et al. Precision of automatic measurements of pigmented skin lesion parameters with a MelaFind(TM) multispectral digital dermoscope. *Melanoma Res.* 2000;10(6):563-570.
13. Gniadecka M, Philipsen PA, Sigurdsson S, et al. Melanoma diagnosis by Raman spectroscopy and neural networks: structure alterations in proteins and lipids in intact cancer tissue. *The Journal of investigative dermatology.* 2004;122(2):443-449.
14. Zonios G, Dimou A, Bassukas I, Galaris D, Tsolakidis A, Kaxiras E. Melanin absorption spectroscopy: new method for noninvasive skin investigation and melanoma detection. *Journal of biomedical optics.* 2008;13(1):014017.
15. Frinking PJ, Bouakaz A, Kirkhorn J, Ten Cate FJ, de Jong N. Ultrasound contrast imaging: current and new potential methods. *Ultrasound in medicine & biology.* 2000;26(6):965-975.
16. Welzel J. Optical coherence tomography in dermatology: a review. *Skin research and technology : official journal of International Society for Bioengineering and the Skin.* 2001;7(1):1-9.
17. Fujimoto JG, Pitris C, Boppart SA, Brezinski ME. Optical coherence tomography: an emerging technology for biomedical imaging and optical biopsy. *Neoplasia.* 2000;2(1-2):9-25.
18. Schmitt JM. Optical coherence tomography (OCT): a review. *Selected Topics in Quantum Electronics, IEEE Journal of.* 1999;5(4):1205-1215.
19. Adabi S, Turani Z, Fatemizadeh E, Clayton A, Nasiriavanaki M. Optical Coherence Tomography Technology and Quality Improvement Methods for Optical Coherence Tomography Images of Skin: A Short Review. *Biomedical engineering and computational biology.* 2017;8:1179597217713475.
20. Leitgeb R, Hitzenberger C, Fercher A. Performance of fourier domain vs. time domain optical coherence tomography. *Optics Express.* 2003;11(8):889-894.
21. Podoleanu AG. Optical coherence tomography. *The British journal of radiology.* 2014.
22. Otis LL, EVERETT MJ, SATHYAM US, COLSTON BW. OPTICAL COHERENCE TOMOGRAPHY: A NEW IMAGING: TECHNOLOGY FOR DENTISTRY. *The Journal of the American Dental Association.* 2000;131(4):511-514.
23. Tearney GJ, Brezinski ME, Bouma BE, et al. In vivo endoscopic optical biopsy with optical coherence tomography. *Science.* 1997;276(5321):2037-2039.
24. Jang I-K, Bouma BE, Kang D-H, et al. Visualization of coronary atherosclerotic plaques in patients using optical coherence tomography: comparison with intravascular ultrasound. *Journal of the American College of Cardiology.* 2002;39(4):604-609.

25. Drexler W, Fujimoto JG. Optical coherence tomography in ophthalmology. *Journal of Biomedical Optics.* 2007;12(4):041201-041201-041202.
26. Drexler W, Fujimoto JG. *Optical coherence tomography: technology and applications.* Springer Science & Business Media; 2008.
27. Schmitt JM, Knuttel A, Yadlowsky M, Eckhaus M. Optical-coherence tomography of a dense tissue: statistics of attenuation and backscattering. *Physics in Medicine and Biology.* 1994;39(10):1705.
28. Thrane L, Frosz MH, Jørgensen TM, Tycho A, Yura HT, Andersen PE. Extraction of optical scattering parameters and attenuation compensation in optical coherence tomography images of multilayered tissue structures. *Optics letters.* 2004;29(14):1641-1643.
29. Schmitt JM, Xiang S, Yung KM. Speckle in optical coherence tomography. *Journal of biomedical optics.* 1999;4(1):95-105.
30. Schmitt J, Xiang S, Yung K. Differential absorption imaging with optical coherence tomography. *JOSA A.* 1998;15(9):2288-2296.
31. Lee P, Gao W, Zhang X. Performance of single-scattering model versus multiple-scattering model in the determination of optical properties of biological tissue with optical coherence tomography. *Applied optics.* 2010;49(18):3538-3544.
32. Levitz D, Thrane L, Frosz M, et al. Determination of optical scattering properties of highly-scattering media in optical coherence tomography images. *Optics express.* 2004;12(2):249-259.
33. Turani Z, Emad F, Avanaki M. Refractive index correction in optical coherence tomography images. Paper presented at: The 23rd Iranian Conference on Optics and Photonics (ICOP 2017) and the 9th Iranian Conference on Photonics Engineering and Technology (ICPET 2017)2017.
34. Avanaki MRN, Podoleanu A. En-face time-domain optical coherence tomography with dynamic focus for high-resolution imaging. *Journal of biomedical optics.* 2017;22(5):56009.
35. Avanaki MRN, Bradu A, Podoleanu A. Optimization of excitation of fiber Fabry-Perot tunable filters used in swept lasers using a phase-correction method. *Applied optics.* 2017;56(12):3378-3382.
36. Nasiri-Avanaki M-R, Hojjatoleslami S, Paun H, et al. Optical coherence tomography system optimization using simulated annealing algorithm. *Proceedings of Mathematical Methods and Applied Computing,(WSEAS, 2009).* 2009:669-674.
37. Boone MA, Suppa M, Dhaenens F, et al. In vivo assessment of optical properties of melanocytic skin lesions and differentiation of melanoma from non-malignant lesions by high-definition optical coherence tomography. *Archives of dermatological research.* 2016;308(1):7-20.
38. Huang D, Swanson EA, Lin CP, et al. Optical coherence tomography. *Science.* 1991;254(5035):1178-1181.
39. Yun S, Tearney G, de Boer J, Iftimia N, Bouma B. High-speed optical frequency-domain imaging. *Optics Express.* 2003;11(22):2953-2963.
40. Goodman JW. *Speckle phenomena in optics: theory and applications.* Roberts and Company Publishers; 2007.
41. Nasiriavanaki M, Xia J, Wan H, Bauer AQ, Culver JP, Wang LV. High-resolution photoacoustic tomography of resting-state functional connectivity in the mouse brain. *Proceedings of the National Academy of Sciences.* 2014;111(1):21-26.
42. Wagner RF, Smith SW, Sandrik JM, Lopez H. Statistics of speckle in ultrasound B-scans. *Sonics and Ultrasonics, IEEE Transactions on.* 1983;30(3):156-163.
43. Hee MR, Izatt JA, Swanson EA, et al. Optical coherence tomography of the human retina. *Archives of ophthalmology.* 1995;113(3):325-332.
44. Magnin PA, von Ramm OT, Thurstone FL. Frequency compounding for speckle contrast reduction in phased array images. *Ultrasonic imaging.* 1982;4(3):267-281.
45. Jørgensen TM, Thrane L, Mogensen M, Pedersen F, Andersen PE. Speckle reduction in optical coherence tomography images of human skin by a spatial diversity method. Paper presented at: European Conference on Biomedical Optics2007.
46. Iftimia N, Bouma BE, Tearney GJ. Speckle reduction in optical coherence tomography by “path length encoded” angular compounding. *Journal of biomedical optics.* 2003;8(2):260-263.
47. Resnikoff HL, Raymond Jr O. *Wavelet analysis: the scalable structure of information.* Springer Science & Business Media; 2012.
48. Wang RK. Reduction of speckle noise for optical coherence tomography by the use of nonlinear anisotropic diffusion. Paper presented at: Biomedical Optics 20052005.
49. Smithies DJ, Lindmo T, Chen Z, Nelson JS, Milner TE. Signal attenuation and localization in optical coherence tomography studied by Monte Carlo simulation. *Physics in Medicine and Biology.* 1998;43(10):3025.
50. Adler DC, Ko TH, Fujimoto JG. Speckle reduction in optical coherence tomography images by use of a spatially adaptive wavelet filter. *Optics letters.* 2004;29(24):2878-2880.
51. Turani Z, Fatemizadeh E, Adabi S, Mehregan D, Daveluy S, Nasiriavanaki M. Noise reduction in OCT skin images. 2017.
52. Adabi S, Mohebbikarkhoran H, Mehregan D, Conforto S, Nasiriavanaki M. An Intelligent Despeckling method for swept source optical coherence tomography images of skin. Paper presented at: SPIE Medical Imaging2017.
53. Adabi S, Rashedi E, Conforto S, Mehregan D, Xu Q, Nasiriavanaki M. Speckle reduction of OCT images using an adaptive cluster-based filtering. *PROGRESS IN BIOMEDICAL OPTICS AND IMAGING.* 2017;10053:100532X.
54. Ozcan A, Bilenca A, Desjardins AE, Bouma BE, Tearney GJ. Speckle reduction in optical coherence tomography images using digital filtering. *JOSA A.* 2007;24(7):1901-1910.
55. Rogowska J, Brezinski ME. Evaluation of the adaptive speckle suppression filter for coronary optical coherence tomography imaging. *Medical Imaging, IEEE Transactions on.* 2000;19(12):1261-1266.
56. Puvanathasan P, Bizheva K. Speckle noise reduction algorithm for optical coherence tomography based on interval type II fuzzy set. *Optics express.* 2007;15(24):15747-15758.
57. Sander B, Larsen M, Thrane L, Hougaard JL, Jorgensen TM. Enhanced optical coherence tomography imaging by multiple scan averaging. *The British journal of ophthalmology.* 2005;89(2):207-212.
58. Kim J, Miller DT, Kim E, Oh S, Oh J, Milner TE. Optical coherence tomography speckle reduction by a partially spatially coherent source. *Journal of Biomedical Optics.* 2005;10(6):064034-064034-064039.
59. Karasakal G, Erer I. Speckle noise reduction in SAR imaging using lattice filters based subband decomposition. Paper presented at: Geoscience and Remote Sensing Symposium, 2007. IGARSS 2007. IEEE International2007.
60. Alsberg BK, Woodward AM, Winson MK, Rowland J, Kell DB. Wavelet denoising of infrared spectra. *Analyst.* 1997;122(7):645-652.
61. Avanaki M, Laissue P, Podoleanu AG, Aber A, Hojjatoleslami S. Evaluation of wavelet mother functions for speckle noise suppression in OCT images. *Int J Graphics Bioinf Med Eng.* 2011;11:1-5.
62. Avanaki M, Laissue P, Podoleanu AG, Hojjatoleslami A. Evaluation of wavelet mother functions for speckle noise suppression in OCT images. *Int J Graphics Bioinfo Med Eng.* 2011;11:1-5.
63. Hwang J-N, Lay S-R, Lippman A. Nonparametric multivariate density estimation: a comparative study. *Signal Processing, IEEE Transactions on.* 1994;42(10):2795-2810.
64. Park H, Miyazaki R, Nishimura T, Tamaki Y. The speckle noise reduction and the boundary enhancement on medical ultrasound images using the cellular neural networks. *電気学会論文誌 C.* 2007;127(10):1726-1731.

65. Bashkansky M, Reintjes J. Statistics and reduction of speckle in optical coherence tomography. *Optics letters.* 2000;25(8):545-547.
66. Adabi S, Conforto S, Clayton A, Podoleanu AG, Hojjat A, Avanaki M. An intelligent speckle reduction algorithm for optical coherence tomography images. Paper presented at: 4th International Conference on Photonics, Optics and Laser Technology, PHOTOPTICS 20162016.
67. Avanaki MR, Laissue PP, Eom TJ, Podoleanu AG, Hojjatoleslami A. Speckle reduction using an artificial neural network algorithm. *Applied optics.* 2013;52(21):5050-5057.
68. Avanaki MR, Laissue PP, Podoleanu AG, Hojjat A. Denoising based on noise parameter estimation in speckled OCT images using neural network. Paper presented at: 1st Canterbury Workshop and School in Optical Coherence Tomography and Adaptive Optics2008.
69. Shankar PM. Speckle reduction in ultrasound B-scans using weighted averaging in spatial compounding. *IEEE transactions on ultrasonics, ferroelectrics, and frequency control.* 1986;33(6):754-758.
70. Pircher M, Go E, Leitgeb R, Fercher AF, Hitzenberger CK. Speckle reduction in optical coherence tomography by frequency compounding. *Journal of Biomedical Optics.* 2003;8(3):565-569.
71. Goodman JW. Some fundamental properties of speckle*. *J Opt Soc Am.* 1976;66(11):1145-1150.
72. Avanaki MR, Cernat R, Tadrous PJ, Tatla T, Podoleanu AG, Hojjatoleslami SA. Spatial compounding algorithm for speckle reduction of dynamic focus OCT images. *Photonics Technology Letters, IEEE.* 2013;25(15):1439-1442.
73. Hecht E, Zajac A. Optics Addison-Wesley. *Reading, Mass.* 1974:301-305.
74. Almasganj M, Adabi S, Fatemizadeh E, et al. A spatially-variant deconvolution method based on total variation for optical coherence tomography images. 2017.
75. Vargas-Martın F, Prieto PM, Artal P. Correction of the aberrations in the human eye with a liquid-crystal spatial light modulator: limits to performance. *JOSA A.* 1998;15(9):2552-2562.
76. Plett ML, Barbier PR, Rush DW. Compact adaptive optical system based on blind optimization and a micromachined membrane deformable mirror. *Appl Opt.* 2001;40(3):327-330.
77. Booth M. Wave front sensor-less adaptive optics: a model-based approach using sphere packings. *Optics Express.* 2006;14(4):1339-1352.
78. Grisan E, Frassetto F, Da Deppo V, Naletto G, Ruggeri A. No wavefront sensor adaptive optics system for compensation of primary aberrations by software analysis of a point source image. 1. Methods. *Appl Opt.* 2007;46(25):6434-6441.
79. Avanaki MR, Long Y, Hojjatoleslami S, Khoshki RM, Podoleanu AG. Fast algorithm for blind optimisation of optical systems; statistics and methodology. *International Journal of Electronics.* 2014;101(9):1179-1189.
80. Nasiri-Avanaki M, Sarmadi H, Meadway A, Podoleanu AG, Hojjatoleslami S. Comparative assessment of three algorithms to control a deformable mirror for an adaptive optics system with no wavefront sensor. Paper presented at: SPIE BiOS2011.
81. Schmitt JM, Liang Z. Deconvolution and enhancement of optical coherence tomograms. Paper presented at: BiOS'97, Part of Photonics West1997.
82. Liu Y, Liang Y, Mu G, Zhu X. Deconvolution methods for image deblurring in optical coherence tomography. *JOSA A.* 2009;26(1):72-77.
83. Kulkarni M, Thomas C, Izatt J. Image enhancement in optical coherence tomography using deconvolution. *Electronics Letters.* 1997;33(16):1365-1367.
84. Ralston TS, Marks DL, Kamalabadi F, Boppart SA. Deconvolution methods for mitigation of transverse blurring in optical coherence tomography. *Image Processing, IEEE Transactions on.* 2005;14(9):1254-1264.
85. Dhawan AP, Rangayyan RM, Gordon R. Image restoration by Wiener deconvolution in limited-view computed tomography. *Appl Opt.* 1985;24(23):4013-4020.
86. Fish D, Walker J, Brinicombe A, Pike E. Blind deconvolution by means of the Richardson–Lucy algorithm. *JOSA A.* 1995;12(1):58-65.
87. Hojjatoleslami S, Avanaki M, Podoleanu AG. Image quality improvement in optical coherence tomography using Lucy–Richardson deconvolution algorithm. *Applied optics.* 2013;52(23):5663-5670.
88. Taghavikhalilbad A, Adabi S, Clayton A, Soltanizadeh H, Mehregan D, Avanaki MRN. Semi-automated localization of dermal epidermal junction in optical coherence tomography images of skin. *Applied optics.* 2017;56(11):3116-3121.
89. Welzel J, Lankenau E, Birngruber R, Engelhardt R. Optical coherence tomography of the human skin. *Journal of the American Academy of Dermatology.* 1997;37(6):958-963.
90. Poulsen T, Wulf HC. Epidermal Thickness at Different Body Sites: Relationship to Age, Gender, Pigmentation, Blood Content, Skin Type and Smoking Habits. *Acta Dermato-Venereologica.* 2003;83(6).
91. Blomgren B, Johannesson U, Bohm-Starke N, Falconer C, Hilliges M. A computerised, unbiased method for epithelial measurement. *Micron.* 2004;35(5):319-329.
92. Hori Y, Yasuno Y, Sakai S, et al. Automatic characterization and segmentation of human skin using three-dimensional optical coherence tomography. *optics express.* 2006;14(5):1862-1877.
93. Hojjatoleslami A, Avanaki MR. OCT skin image enhancement through attenuation compensation. *Applied optics.* 2012;51(21):4927-4935.
94. Zhang J, Nelson JS, Chen Z. Removal of a mirror image and enhancement of the signal-to-noise ratio in Fourier-domain optical coherence tomography using an electro-optic phase modulator. *Optics letters.* 2005;30(2):147-149.
95. Bohren CF, Huffman DR. *Absorption and scattering of light by small particles.* John Wiley & Sons; 2008.
96. Lutomirski R, Yura H. Propagation of a finite optical beam in an inhomogeneous medium. *Appl Opt.* 1971;10(7):1652-1658.
97. Goodman JW. to Fourier Optic. *Mac Graw-Hill, New York.* 1960.
98. Yura HT, Hanson SG. Optical beam wave propagation through complex optical systems. *JOSA A.* 1987;4(10):1931-1948.
99. Yura HT, Thrane L, Andersen PE. Closed-form solution for the Wigner phase-space distribution function for diffuse reflection and small-angle scattering in a random medium. *JOSA A.* 2000;17(12):2464-2474.
100. Born M. E. Wolf Principles of optics. *Pergamon Press.* 1980;6:188-189.
101. Levitz D, Andersen CB, Frosz MH, et al. Assessing blood vessel abnormality via extracting scattering coefficients from OCT images. Paper presented at: European Conference on Biomedical Optics 20032003.
102. Thrane L, Yura HT, Andersen PE. Analysis of optical coherence tomography systems based on the extended Huygens–Fresnel principle. *JOSA A.* 2000;17(3):484-490.
103. Andersen PE, Thrane L, Yura HT, Tycho A, Jørgensen TM, Frosz MH. Advanced modelling of optical coherence tomography systems. *Physics in medicine and biology.* 2004;49(7):1307.
104. Avanaki M, Podoleanu AG, Schofield JB, et al. Quantitative evaluation of scattering in optical coherence tomography skin images using the extended Huygens–Fresnel theorem. *Appl Opt.* 2013;52(8):1574-1580.
105. Avanaki MR, Podoleanu AG, Price MC, Corr SA, Hojjatoleslami S. Two applications of solid phantoms in performance assessment of optical coherence tomography systems. *Applied optics.* 2013;52(29):7054-7061.

106. Hughes M, Podoleanu AG. Simplified dynamic focus method for time domain OCT. *Electronics letters.* 2009;45(12):623-624.
107. Avanaki MR, Hojjatoleslami A, Sira M, Schofield JB, Jones C, Podoleanu AG. Investigation of basal cell carcinoma using dynamic focus optical coherence tomography. *Applied optics.* 2013;52(10):2116-2124.

List of figure captions:

Fig 1 Simplified configuration of a time-domain OCT system

Fig 2 Block diagram of de-speckling algorithm based on artificial neural network

Fig 3 A B-scan image acquired from a 25 years-old male cheek, (a) original image (b) de-speckled image

Fig 4 Spatial compounding de-speckling algorithm

Fig 5 Image debluring using deconvolution, (a) original image of skin of palm taken from a 25 years-old male, (b) de-speckled image. The arrows indicate areas of improvement.

Fig 6 Flowchart of attenuation compensation for OCT skin images

Fig 7 Preprocessing and attenuation compensation of OCT fingertip images (a) de-speckled image (b) skin layers' borders (c) attenuation compensated image

Fig 8 Comparison between scattering coefficients obtained using Mie theory and those from OPE algorithm

List of figures:

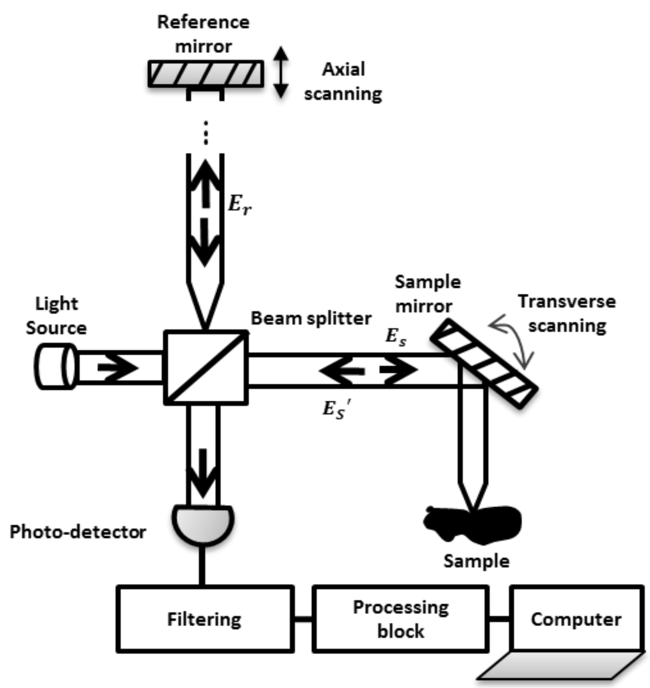

Fig 1 Simplified configuration of a time-domain OCT system

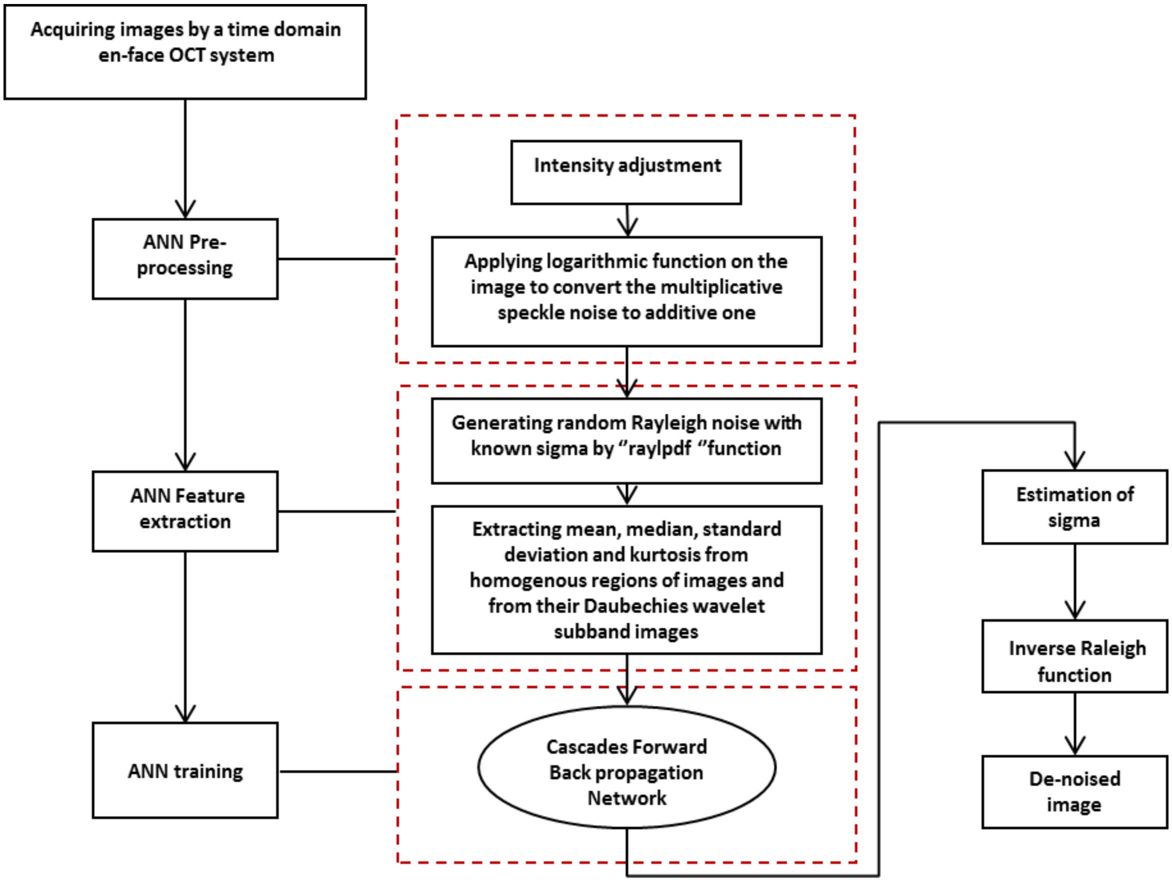

Fig 2 Block diagram of de-speckling algorithm based on artificial neural network

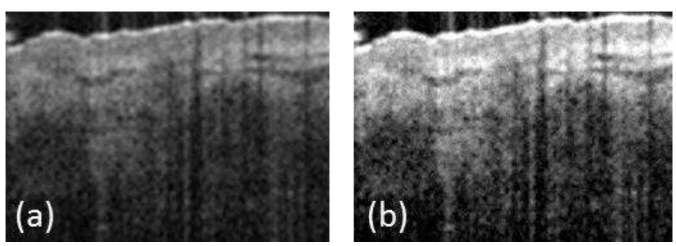

Fig 3 A B-scan image acquired from a 25 years-old male cheek, (a) original image (b) de-speckled image

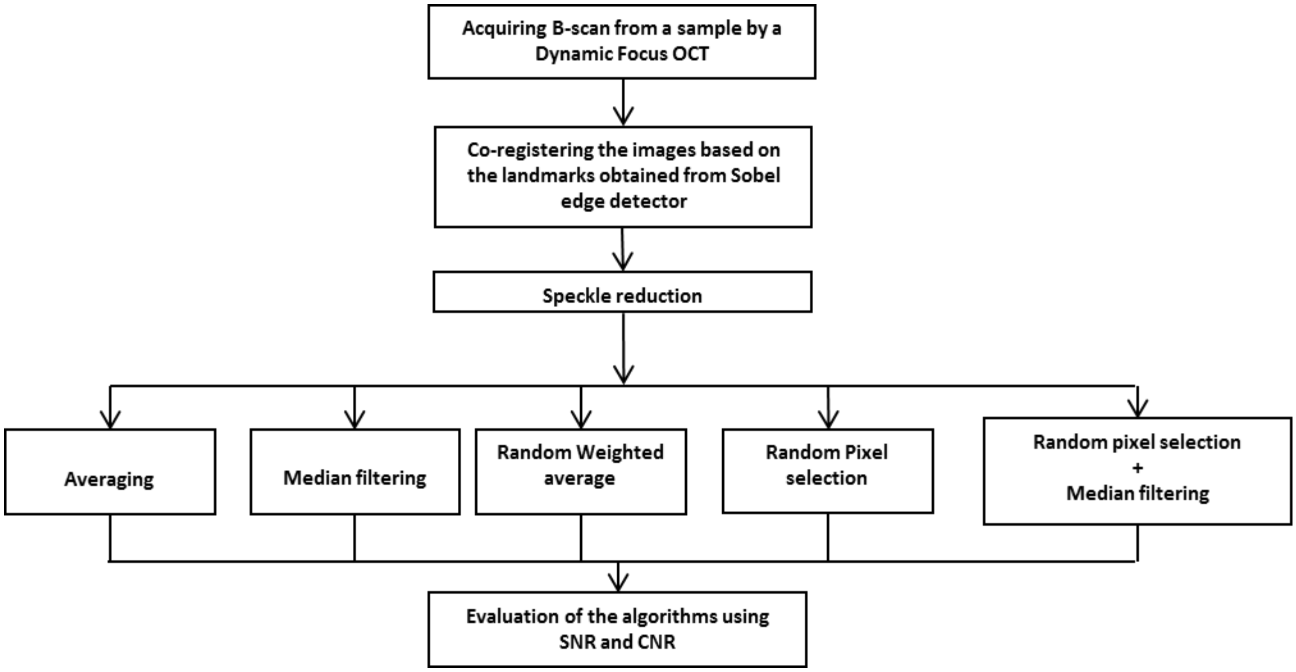

Fig 4 Spatial compounding de-speckling algorithm

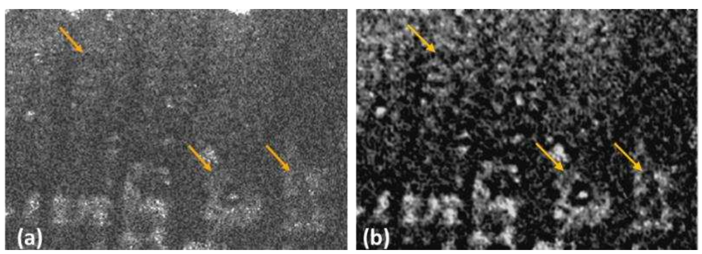

Fig 5 Image debluring using deconvolution, (a) original image of skin of palm taken from a 25 years-old male, (b) de-speckled image. The arrows indicate areas of improvement.

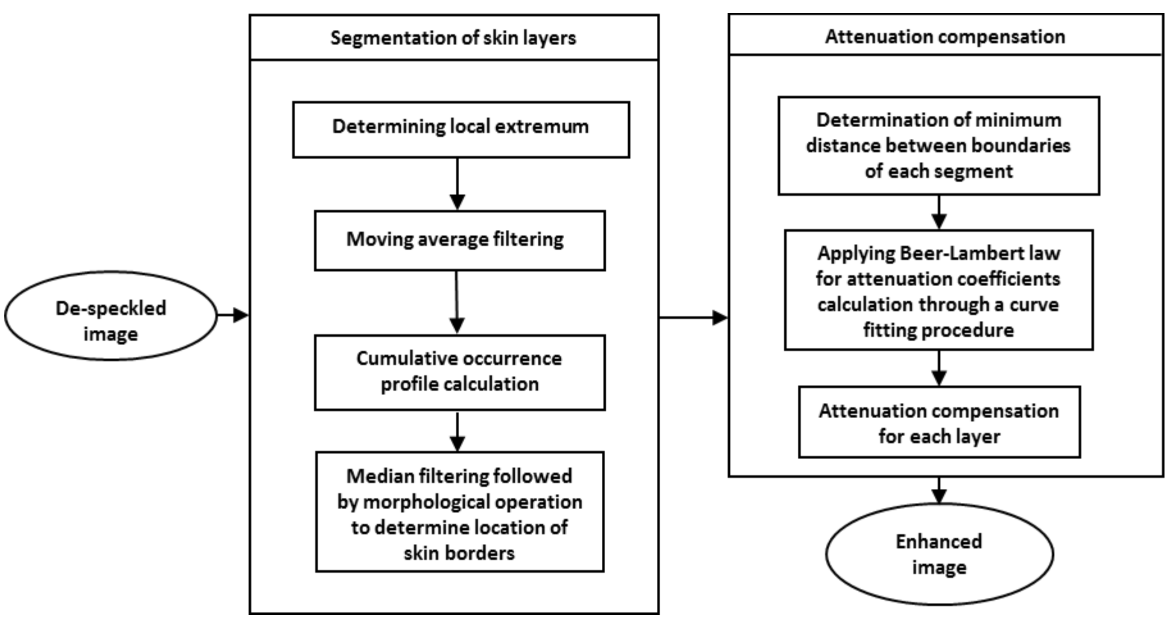

Fig 6 Flowchart of attenuation compensation for OCT skin images

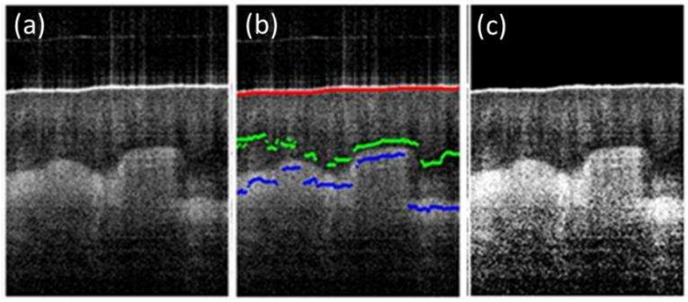

Fig 7 Preprocessing and attenuation compensation of OCT fingertip images (a) de-speckled image (b) skin layers' borders (c) attenuation compensated image

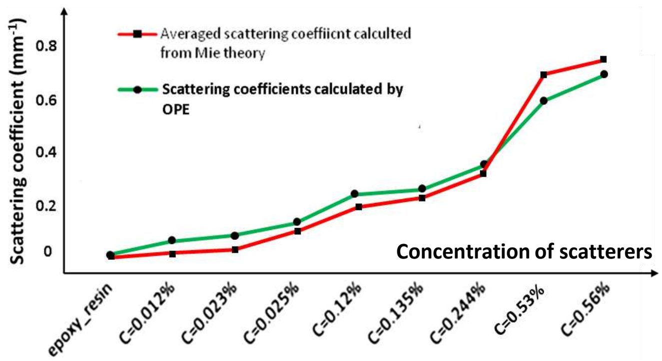

Fig 8 Comparison between scattering coefficients obtained using Mie theory and those from OPE algorithm